

Early in-flight detection of SO₂ via Differential Optical Absorption Spectroscopy: a feasible aviation safety measure to prevent potential encounters with volcanic plumes

L. Vogel¹, B. Galle², C. Kern^{1,*}, H. Delgado Granados³, V. Conde², P. Norman², S. Arellano², O. Landgren², P. Lübcke¹, J. M. Alvarez Nieves³, L. Cárdenas Gonzáles⁴, and U. Platt¹

¹Institute of Environmental Physics, University Heidelberg, Heidelberg, Germany

²Department of Earth and Space Sciences, Chalmers University of Technology, Gothenburg, Sweden

³Instituto de Geofísica, UNAM, Mexico D. F., Mexico

⁴Centro Nacional de Prevención de Desastres, Mexico D. F., Mexico

* now at: Cascades Volcano Observatory, US Geological Survey, Vancouver, WA, USA

Received: 5 May 2011 – Published in Atmos. Meas. Tech. Discuss.: 16 May 2011

Revised: 7 August 2011 – Accepted: 22 August 2011 – Published: 8 September 2011

Abstract. Volcanic ash constitutes a risk to aviation, mainly due to its ability to cause jet engines to fail. Other risks include the possibility of abrasion of windshields and potentially serious damage to avionic systems. These hazards have been widely recognized since the early 1980s, when volcanic ash provoked several incidents of engine failure in commercial aircraft. In addition to volcanic ash, volcanic gases also pose a threat. Prolonged and/or cumulative exposure to sulphur dioxide (SO₂) or sulphuric acid (H₂SO₄) aerosols potentially affects e.g. windows, air frame and may cause permanent damage to engines. SO₂ receives most attention among the gas species commonly found in volcanic plumes because its presence above the lower troposphere is a clear proxy for a volcanic cloud and indicates that fine ash could also be present.

Up to now, remote sensing of SO₂ via Differential Optical Absorption Spectroscopy (DOAS) in the ultraviolet spectral region has been used to measure volcanic clouds from ground based, airborne and satellite platforms. Attention has been given to volcanic emission strength, chemistry inside volcanic clouds and measurement procedures were adapted accordingly. Here we present a set of experimental and model results, highlighting the feasibility of DOAS to be used as an airborne early detection system of SO₂ in two spatial dimensions. In order to prove our new concept, simultaneous airborne and ground-based measurements of the plume of Popocatepetl volcano, Mexico, were conducted

in April 2010. The plume extended at an altitude around 5250 m above sea level and was approached and traversed at the same altitude with several forward looking DOAS systems aboard an airplane. These DOAS systems measured SO₂ in the flight direction and at ± 40 mrad (2.3°) angles relative to it in both, horizontal and vertical directions. The approaches started at up to 25 km distance to the plume and SO₂ was measured at all times well above the detection limit. In combination with radiative transfer studies, this study indicates that an extended volcanic cloud with a concentration of 10¹² molecules cm⁻³ at typical flight levels of 10 km can be detected unambiguously at distances of up to 80 km away. This range provides enough time (approx. 5 min) for pilots to take action to avoid entering a volcanic cloud in the flight path, suggesting that this technique can be used as an effective aid to prevent dangerous aircraft encounters with potentially ash rich volcanic clouds.

1 Introduction

Volcanic gaseous emissions are typically composed of carbon dioxide (CO₂), water vapour, sulphur dioxide (SO₂), and halogen compounds. Depending on the conditions the plumes/clouds can also contain large amounts of ash (i.e. small, solid particles). A series of life threatening encounters of aircraft with ash-loaded volcanic clouds in the 1980s highlighted the risk of volcanic emissions to aviation. The main threat is posed by volcanic ash (Miller and Casadevall, 2000; ICAO, 2007; Prata and Tupper, 2009, and



Correspondence to: L. Vogel
(leif.vogel@iup.uni-heidelberg.de)

references therein), which may lead to engine failure via flame-outs if allowed to enter high temperature jet engines. Severe incidents were reported from Mt. St. Helens 1980, where a Lockheed C-130 lost two of its four turboprop engines; in the 1982 eruption of Galunggung, Indonesia, two Boeing 747 lost power in one case of all four, in the other of three out of four engines at 11 300 m and 9000 m above sea level (a.s.l.), respectively. The crew of both airplanes managed to restart enough engines to make a safe landing at nearby airports, but only after descending several kilometres. A similar encounter occurred in 1989, when a Boeing 747 flew into the cloud from nearby Redoubt volcano, Alaska, and lost power of all of its four engines (Casadevall, 1994). Also in this case, the crew managed to restart the engines one or two minutes prior to impact on the ground. Fortunately only economic losses resulted from these encounters and no human lives were lost. The eruption of Mt. Pinatubo 1991 resulted in more than 40 incidents, but none as dramatic as the above-mentioned ones. Nevertheless, damage to aircraft as a result of the Mt. Pinatubo eruption were estimated to exceed US\$ 100 million (Miller and Casadevall, 2000).

Even encounters with volcanic clouds of relatively low ash and SO₂ content may have severe consequences to aircraft. Grindle and Burcham (2003) describe an incident in August 2000, where a DC-8-72 research airplane of NASA flew into a volcanic cloud of Hekla volcano, Iceland. The presence of a volcanic plume was only verified afterwards by the scientific in-situ instruments on-board the airplane. No signs of a volcanic cloud were perceived by the crew. Although no damage was revealed by a first visual inspection of the engines, a later inspection showed that significant damage to the engines had occurred with clogged cooling passages of turbine blades and SO₂ in the engine oil. It was estimated that the remaining lifetime of certain vital parts of the engine was likely reduced to only about 100 h.

The incidents described above resulted from the melting point of volcanic ash (≈ 1100 K) being below typical operational temperature (1400 K) of jet engines if thrust is above idle. This can lead to clogging and accumulation of molten debris in the hotter part of the engine and its consequent loss of power. Other effects include clogging of cooling mechanisms which greatly reduces the engines' lifetime, and abrasion of engine parts. Next to its effects to the engines, the abrasive properties of volcanic ash can damage the outer hull of aircraft, avionic systems e.g. pitot-static tubes and abrade windscreens to the point of becoming opaque. Besides volcanic ash, certain volcanic gases can also be hazardous to aviation, especially sulphur dioxide SO₂ and sulphuric acid H₂SO₄. Although they do not impair the airworthiness of an aircraft in such drastic ways as volcanic ash, prolonged exposure might reduce the lifetime of aircraft systems and lead to costly repairs and ground time of the aircraft (Bernard and Rose, 1990; ICAO, 2007).

One of the latest volcanic eruptions severely impacting commercial aviation was the April/May 2010 eruption of

Eyjafjallajökull in April 2010 with a volcanic cloud being blown over Europe. Most of European airspace was closed for up to several weeks and although no life-threatening encounters occurred, economic losses are estimated to range up to € 2.5 billion for the airline industry alone (Zehner, 2010). This eruption demonstrated the vulnerability of modern societies to volcanic hazards. In the course of the Eyjafjallajökull crisis, the “no-fly-rule”, which states that aircraft are not allowed to fly through volcanic clouds of any ash concentration, was replaced by conditional flying zones. The “No Fly Zone” encompasses areas with ash concentration higher than $2 \times 10^{-3} \text{ g m}^{-3}$ and the “Enhanced Procedures Zone”, where volcanic ash concentrations are predicted to be between 2×10^{-4} and $2 \times 10^{-3} \text{ g m}^{-3}$. This more flexible approach was meant to keep European air-traffic operational, but also has the risk of reduced life times of aircraft parts. Also, this new approach places new and more demanding necessities for modelling on the volcanic advisory centres (VAACs), because a much more detailed initiation of models, knowledge of source terms, and incorporation of all physical processes are necessary (ADF, 2010).

Commercial carriers rely on the volcanic ash advisory centres (VAACs) of the International Airways Volcano Watch (IAVW) for volcanic cloud warnings and predicted locations of these clouds (Romero, 2004; ICAO, 2007). The VAACs use a wide set of observations and measurements, including ground based measurements from observing networks, special air-reports from pilots and observations from satellites (meteorological and non-meteorological). Most active volcanoes are not routinely monitored. Even if they are in remote locations, they can be in close proximity to busy air routes e.g. the Aleutian islands (Kasatochi volcano) and volcanoes in Kamchatka for trans-Pacific air routes. Furthermore, volcanic ash ejected into higher atmospheric layers can be rapidly dispersed over great distances (Prata, 2009), and eruption strength is not directly linked to ejection height (Tupper et al., 2009). Satellite based measurements of ash and SO₂ are thus the most important tool to detect volcanic clouds and eruptions (Prata, 2009; Thomas and Watson, 2010).

Ash detection from satellite platforms can be accurately performed in the infra-red (IR) spectral region. Retrievals are typically based on the “reverse absorption”, the different absorption structures of water and ice versus ash in the 10 to 13 μm range, by taking the difference of these absorption structures (“brightness temperature difference (BTD) method”, Prata, 1989; Wen and Rose, 1994). In recent years the addition of further channels in the retrievals has improved the detection limit and the ability to identify volcanic ash (e.g. Pavolonis et al., 2006; Pavolonis and Sieglaff, 2010; Clarisse et al., 2010; Thomas and Watson, 2010, and references therein). While pure ash clouds can be distinguished from water/ice clouds, mixed clouds are more difficult to separate. Volcanic dust clouds can also be masked by “ordinary” meteorological clouds, and artefacts associated with

dust or very cold cloud tops can cause false detections. These limitations have been discussed extensively and are known to the community (Prata, 1989; Rose et al., 1995; Simpson et al., 2000; Prata et al., 2001). With the introduction of high resolution instruments like Infrared Atmospheric Sounding Interferometer (IASI) and Atmospheric Infrared Sounder (AIRS), false ash detection induced by dust can be reduced significantly (Clarisse et al., 2010).

In the context of volcanic aviation hazards, SO₂ detection is used as a supplementary technique, because volcanic ash clouds are usually associated with SO₂ clouds of approximately equal size and location. SO₂ can be identified by its molecular absorption structures, both in the UV and IR spectral regions, the extent of a SO₂ cloud can serve as an indicator for areas affected by volcanic ash. Typically SO₂-levels in the free troposphere are very low (< 100 ppt above 2 km, Berglen et al., 2004), therefore there is only a very small background signal. Detection in the IR is mainly based on SO₂ absorptions bands around 7.3 μm (Prata et al., 2003; Prata and Bernardo, 2007), the 8.6 μm (Realmuto et al., 1994), and recently was combined with the 4 μm band (Karagulian et al., 2010). Remote sensing of SO₂ in the ultraviolet (UV) range is more sensitive and this region has been used since 1977 (COSPEC and later TOMS, see for instance Krueger, 1983). Today retrievals of SO₂ are based on Differential Optical Absorption Spectroscopy Technique (DOAS) (e.g. Platt and Stutz, 2008), and satellite-based SO₂ detection has proven very useful in detecting and tracking volcanic plumes in several cases in the past (Khokhar et al., 2005, 2008; Rix et al., 2009; Carn et al., 2009). Although reliable, the major drawback of volcanic SO₂ detection in the UV range is its limitation to daylight and limited coverage/overpass. Also, it can only be a proxy for the greater hazard, volcanic ash, which will fall out and might lead to two different clouds moving in different directions due to wind shear. However, for young clouds (up to three days after emission) SO₂ remains a good tracer for a volcanic cloud with dangerous ash contents (Carn et al., 2009; Guffanti et al., 2010; Schumann et al., 2011; Thomas and Prata, 2011). Even if most of the ash and SO₂ have separated, the SO₂ cloud might still contain fine ash particles (Thomas and Prata, 2011).

Detection of a volcanic eruption that potentially poses a danger to aviation should in the best case lead to a warning to aircraft within minutes. However, if the eruption goes unnoticed because the volcano is in a remote location, the weather conditions are unfavourable for satellite detection, or the satellite overpass misses it, several hours might pass before the threat is recognized and warning can be given. Thus already Prata et al. (1991) proposed an instrument on board aircraft to sense volcanic ash by its IR emission signature. A portable camera applicable for this purpose was presented in Prata and Bernardo (2009). The maximum detection range of such a system is ≈100 km (Barton and Prata, 1994).

Although cameras for the detection of SO₂ based on two-wavelength detection in the UV range exist since 2006 (Mori and Burton, 2006; Dalton et al., 2009; Kantzas et al., 2010; Bluth et al., 2007; Kern et al., 2010a), detection limits reported to date are of the order of 10¹⁷ molec cm⁻² SO₂ slant column densities (SCDs) (Mori and Burton, 2006; Lübcke, 2010). This is not sufficient to detect expected SO₂ SCDs measured at greater distances to the volcanic cloud, as will be shown in this study. Remote sensing with the DOAS technique is more specific and offers better sensitivity than two-wavelength detection schemes.

In the following we will explore the feasibility of the DOAS technique as central component of an early in flight warning system of SO₂ and hence volcanic plumes. Prototype systems were tested, during a flight of a small airplane with forward looking DOAS instruments mounted. The volcanic plume of Popocatepetl was approached several times. Popocatepetl volcano is a suitable candidate for this test, because its summit is at a height of 5426 m (a.s.l.) while the elevation of the surrounding terrain is around 2000 m a.s.l. With the planetary boundary layer extending to an altitude of 2500–3000 m above ground (Doran et al., 1998), the plume disperses usually outside the planetary boundary layer at heights comparable to low flying commercial aircraft. Reported average emissions during April 2010 were of about 20 kg s⁻¹ (1.730 Gg d⁻¹) according to the measurements of local monitoring stations from the Network for Observation of Volcanic and Atmospheric Change (NOVAC).

The paper is structured as follows: the general concept of an early in-flight detection system for SO₂ based on the DOAS technique is presented in Sect. 2. Section 3 describes the experimental setup used to proof the concept and the performed airborne measurements as well as additional ground based measurements. Also, the retrieval of SO₂ from gathered spectra is given. Radiative transfer studies performed with the conditions at hand are introduced. Subsequently, the results are discussed in Sect. 4. Experimental data is compared with radiative transfer studies to infer the maximum distance for detecting SO₂ in Sect. 5. The results of this study are concluded in Sect. 6. An analytical description of the expected decrease of SO₂ signal with distance is derived in Appendix A.

2 Early in-flight detection of SO₂ via Differential Optical Absorption Spectroscopy

Airborne DOAS measurements are routinely performed from various research aircraft. Recent examples from CARIBIC (Civil Aircraft for Regular Investigation of the atmosphere Based on an Instrument Container) of observations of volcanic plumes are described in Heue et al. (2011), which measured volcanic clouds originating from Kasatochi (2008), and Eyjafjallajökull (2010). Different trace gases could be identified (BrO, SO₂). These measurements were performed

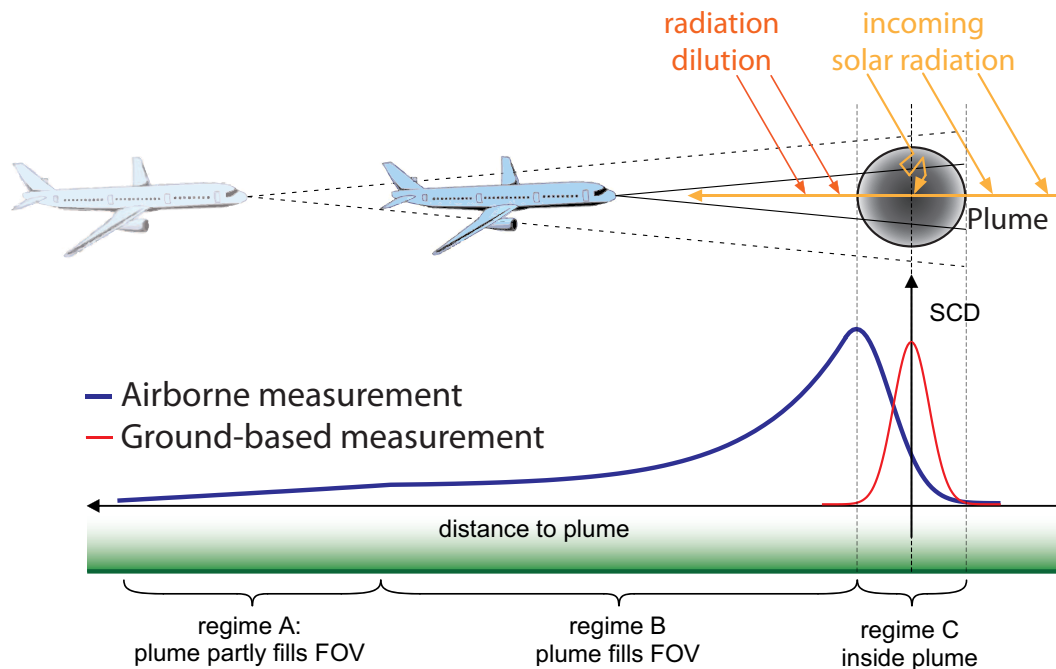


Fig. 1. Upper part: sketch of observation geometry of a forward looking telescope in an aircraft approaching a volcanic plume. There are three regimes: A – the plume only partly fills the field of view (FOV) of the instrument, B – the plume completely fills the FOV, C – the instrument is inside the plume. Lower part: SO₂ SCD seen by aircraft based (blue line) and ground based instruments (red line). Details see text.

with sideways looking instruments and interest was focused on satellite validation and plume chemistry. Here, we explicitly study the capabilities of a forward looking DOAS instrument as an early warning system for SO₂.

Figure 1 illustrates the SO₂ signal to be expected from a forward looking telescope mounted in an airplane. In the upper part, it shows a sketch of the observation geometry for a forward looking telescope in an aircraft approaching a volcanic plume and in the lower part the expected SO₂ slant column densities (SCDs) for an airborne approach traversing through the plume as well as for a ground-based, upward looking instrument (e.g. an instrument mounted on a car) traversing beneath the plume. A gaussian distribution of the SO₂ concentration in the plume is assumed. Also indicated are three regimes for airborne approaches: A – the plume only partly fills the field of view (FOV) of the instrument, B – the plume completely fills the FOV, C – the measurements are performed inside the plume. In regime A there is a strong increase of the SO₂ SCD with decreasing distance to the plume for two reasons, (1) as the instrument approaches the plume continues to fill a larger part of the FOV, (2) less radiation is scattered into the FOV between the instrument and the plume. The radiation from the FOV not having penetrated the plume does not carry the SO₂ absorption signature, thus, both effects will lead to increase of the SO₂ optical density seen by the instrument at smaller distances to the plume. Once

the volcanic plume fills the FOV of the instrument (regime B), increase in SO₂ absorption structure with decreasing distance should follow an exponential increase with a subsequent drop in retrieved SO₂ signal inside the plume. It is interesting to note that (for an optically thin plume with little multiple scattering inside) the airborne measurements will see the maximum SO₂ SCD when the aircraft (and thus the instrument) reaches the front edge of the plume. Ground-based instruments will see the maximum SO₂ SCD when the instrument is just below the plume centre. As our radiative transfer study (Sect. 3.4) and measured data (Sect. 3) show in this study, the exact gradient seen by an instrument inside the plume depends on the aerosol load at hand. Also, the maximum SO₂ SCD might be perceived not at the edge but further inwards in the plume for airborne approaches.

In order to take evasive measures and prevent an encounter of the aircraft with a volcanic cloud, the above described approach of an instrument looking along the direct flight vector needs to be extended to resolve the plume spatially. This is easily achieved by additional instruments with viewing directions along a horizontal and vertical offset to the flight vector. In the best case this would result in displaying a two dimensional distribution of SO₂ SCDs in the direction of flight of the aircraft (see Sect. 3), allowing to circumvent areas of increased SO₂ concentration and minimizing the chance to encounter volcanic ash by evasive action.



Fig. 2. A schematic of the different airborne viewing directions. All telescopes were mounted at the airplane close to co-pilots window. The viewing directions (up, down, starboard, port) were looking at angles of 40 mrad with respect to centre and a horizontal plane (up, down) or a vertical plane (starboard, port).

An additional radiative transfer study was conducted to reproduce the measurements, extrapolate found dependencies to greater distances and infer the limit of detectability of the plume.

3 Experimental setup

In order to provide experimental proof of our concept for a DOAS-based early warning system, we performed measurements on board a small airplane probing the plume of Popocatepetl volcano, Mexico, on 24 April 2010. As mentioned above, Popocatepetl is especially well suited for studies on the detection of SO₂ from airplanes due to (1) its high altitude of 5426 m a.s.l. and its relatively high SO₂ emission flux. Moreover (2), Popocatepetl is one of the volcanoes, which are equipped with ground-based DOAS instrumentation for continuous monitoring of the SO₂ emission flux within the NOVAC network (Galle et al., 2010), thus independent measurements of the SO₂ emission were available, which were – according to the ground-based network – around 1.9 Gg day⁻¹ during the time of our measurements. Also, plume height and direction were monitored by two additional ground based stationary scanning instruments and conventional car traverses of the plume were conducted with a zenith sky looking DOAS instrument. (3) These flights provided a largely realistic simulation of an encounter with an arbitrary volcanic plume in the troposphere outside of the planetary boundary layer (PBL) as e.g. encountered during the Eyjafjallajökull eruption over Europe during April and May 2010.

The meteorological conditions were stable with clear visibility at flight altitude for all approaches. An open cloud cover well above the plume was present as well as a slight haze in the boundary layer below.

The airborne measurements were conducted with a Cessna 421, on which three telescopes were installed next to the window of the copilot. One telescope was pointing directly forward at 0 mrad elevation angle, where as the other two

Table 1. Spectrographs used for airborne measurements, their respective viewing direction in mrad from centre and detection limits (95 % = $2 \times \sigma$). σ is the mean error of all measurements with distance greater than 10 km to the plume of approaches III–V for the respective instrument.

Spectrograph model	viewing direction [mrad]	SO ₂ [10 ¹⁶ molec cm ⁻²] detec. limit	σ
QE65000	0	centre	1.6
S2000	40	up	2.9
S2000	40	down	2.8
S2000	40	port	2.6
S2000	40	starboard	2.9

were dual beam telescopes similar to the ones described in Johansson et al., 2009. Each dual beam telescope has two viewing directions separated by 80 mrad (4.6°). These telescopes were aligned such that they were pointing 40 mrad (2.3°) towards port and starboard and 40 mrad above and below the central viewing direction, respectively (Fig. 2). Each of the three telescopes was connected to a spectrometer (or two in the case of the dual beam telescopes) with which the incident light was spectrally analysed. The fibre from the centre looking telescope was connected to a high grade spectrograph (QE65000, Ocean Optics), light from the sideways looking dual-beam telescopes was analysed with dual spectrograph of type S2000 (Ocean Optics) with (compared to the QE65000 instrument) somewhat lower resolution and higher noise (Table 1). The field of view (FOV) for all five viewing directions was 8 mrad (0.46°). In this way, the setup was able not only to detect the volcanic plume but also gather information on its spatial extent. The instrumental setup was very compact with telescopes of size 115 mm × 40 mm (length × diameter) and spectrograph dimensions (length × width × height) of 141.6 mm × 104.9 mm × 40.9 mm (S2000) and 182 mm × 110 mm × 47 mm (QE65000).

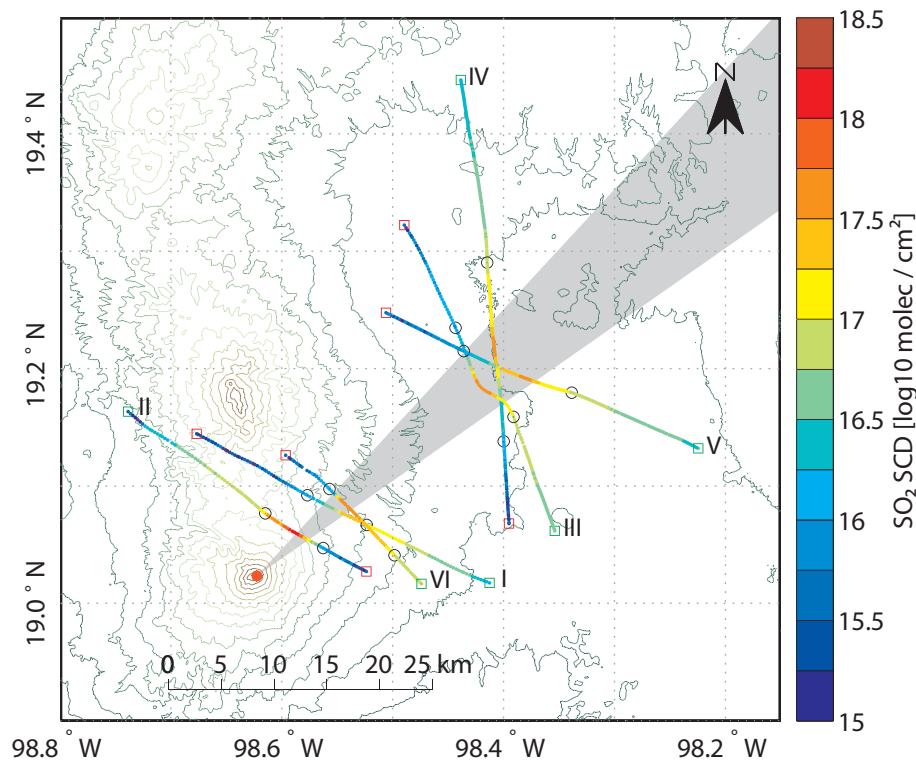


Fig. 3. Map of all six flown approaches. The start of each approach is marked by a green square, the end by a red square. The roman numbers next to the starting point correspond to the chronological order of the different approaches. Note the logarithmic colour scale of the SO₂ SCDs. Popocatepetl is indicated with an orange dot at the lower left corner and its plume by the grey shaded area.

3.1 Airborne measurements

In total, six approaches towards and subsequent traverse through the volcanic plume were made between 16:00 h and 17:15 h UTC. They are labelled I till VI in Fig. 3. Further information on average altitude a.s.l. and direction of approach [azimuth °N] are given in Table 2. The azimuth and elevation angles were calculated from the GPS data recorded on board the aircraft. Thus both values represent viewing direction based on the difference between two subsequent locations of measurement and can only be approximates for the planes orientations yaw, pitch and actual viewing direction of the telescopes.

The purpose of approaches I and II was to gather information about the plume altitude and to test the instrumental setup before going to greater distances from the plume. Like approach VI, they are not well suited for studying the detectability of SO₂ due to the encounter of strong inhomogeneities in the plume, or since the aircraft flew at the wrong altitude and/or changes in flight course had to be made. The effect of a misaligned approach of the plane can be seen e.g. in approach II, where a change in the plane's approach elevation angle was associated with a sudden increase in the SO₂ column density measured by the central DOAS instru-

Table 2. Mean altitude a.s.l. and azimuth direction from north for all plane approaches. Approaches marked by (*) are not used for the study e.g. due to variability in flight direction during approach or insufficient distance to the plume. Approach II (+) with stable flight vector inside the plume is only used for comparison between ground based and airborne measurements (Sect. 4.1).

Approach	Time [UTC]	Altitude [m]	Azimuth [°N]
I*	15:58–16:03	5067	297
II ⁺	16:06–16:11	5184	124
III	16:15–16:21	5197	334
IV	16:24–16:31	5186	174
V	16:42–16:49	5207	293
VI*	17:09–17:13	5546	314

ment (Fig. 8). While this approach can not be used to study DOAS as an early detection technique of SO₂, it still allows comparison with the car traverse (Sect. 4.1). Approaches III, IV and V were conducted starting at larger distance to the plume and will be discussed in detail in the following. Due to air space restrictions the maximum distance to the plume achieved at the start of an approach was only 25 km or less. To draw conclusions about the maximum distance at which

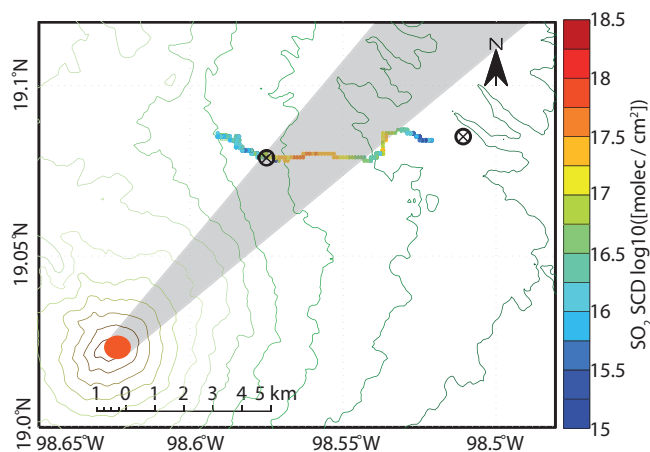


Fig. 4. Ground based measurements: an example of conducted car traverses is shown with measured SO₂ SCDs on a logarithmic scale. The locations of the stationary scanning instruments are marked by black circles. Popocatepetl as a source is indicated with an orange dot at the lower left corner and its plume by the grey shaded area.

SO₂ from the plume might still be detected, the measurements need to be extrapolated using theoretical considerations (Appendix A) as well as radiative transfer model studies (Sect. 5).

3.2 Ground based measurements

Further measurements were conducted from the ground to provide plume altitude and wind direction. These parameters were communicated to the airplane via radio link. A zenith pointing DOAS instrument was mounted on a car and used to conduct traverse measurements under the plume between 8 and 14 km distance to the crater, yielding location and extent of the plume as well as wind direction (Fig. 4). Because of road conditions and construction along the way, traversing the plume generally took about one hour. Also, the plume was not blown perpendicular to the road. Calculation of fluxes and wind direction was performed using the MobileDOAS software package (Zhang and Johansson, 2007).

Additionally, two stationary DOAS instruments were deployed on both edges of the plume (Fig. 4), allowing to approximate wind direction as well as the plume altitude. The instrumental design is analogue to the NOVAC instrument Version I as described in Galle et al. (2010). They scan the volcanic plume along a 60° cone, which is a routinely performed volcanic gas emission measurement technique in the NOVAC network. Calculation of plume height and direction was also performed with the NOVAC software package. The stationary instruments had the advantage of a higher time resolution (≈ 10 min per scan) than the traverses.

3.3 The DOAS retrieval

All gathered spectra were evaluated using the DOASIS software package from the Institute for Environmental Physics, Heidelberg, Germany (Doasis; Kraus, 2006; Lehmann, 2011). The program applies a combination of a non-linear Levenberg-Marquardt and a standard least-squares fit to determine the optical density of trace gas absorption (Platt and Stutz, 2008). Absorption cross sections of the following species were included in the fit: SO₂ at 273 K (Bogumil et al., 2003) and O₃ at 280 K (Voigt et al., 2001), both chosen for their close vicinity to ambient temperature at the flight height. In addition to SO₂ and O₃, also a clear sky reference (CSR) spectrum and a Ring spectrum (Solomon et al., 1987) were fitted. The latter was calculated from the CSR with the software DOASIS. Broad band absorptions and Mie scattering were accounted for by using a polynomial of 3rd order and a wavelength-independent offset was included to correct for possible stray light. All spectra collected were evaluated in the wavelength range between 307.4–317.8 nm. For all instruments and approaches of the airborne measurements, CSR spectra were constructed from 10 consecutively recorded spectra, measured after the plane had passed the plume but still continued on the same course. Thus the CSR was recorded under as similar as possible illumination conditions as the actual measurements and in close temporal proximity. The CSR was wavelength calibrated by comparison to a high resolution solar spectrum (Kurucz, 2005), which was convoluted with the respective instrumental slit function. The obtained calibrations were transferred to all other spectra of corresponding approach and instrument. The ambient temperature at flight altitude was approximately -1 °C according to data from the READY NOAA model (READY) at 500 mbar or 5120 m a.s.l. at the time of the flight on 24 April 2010.

Note that in contrast to previous radiative transfer studies (Mori et al., 2006; Kern et al., 2010b), here we do not aim to retrieve correct SO₂ SCDs but intent only to study the gradient of the SO₂ signal with distance to the plume. Thus the evaluation of gathered data in this fit range most sensitive to SO₂ is justified. A correction factor of 2 was used to calculate the measurement error from the fit error according to (Platt and Stutz, 2008) based on residual structures and SO₂ absorption band widths. The mean measurement error is determined from all measurements gathered at distances greater than 10 km for approaches III–V of the respective instrument (Table 1). In this way, the error reflects uncertainties of measurements at greater distance to the plume.

3.4 Radiative transfer modelling

Several model scenarios were set up in the 3-D radiative transfer model McArtim (Deutschmann, 2008; Deutschmann et al., 2011), successor of the model TRACYII (Wagner et al., 2007), to assess the sensitivity of DOAS measurements

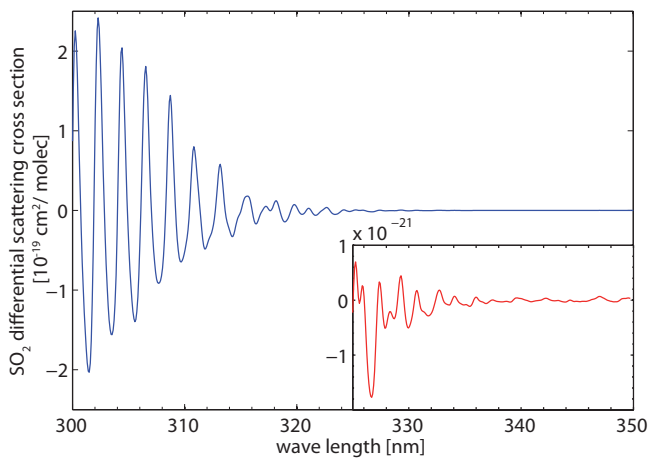


Fig. 5. A high pass filtered SO₂ cross section at the same optical resolution as the QE65000 spectrograph used with the centre looking telescope. The inserted graph displays the respective part of the SO₂ cross section magnified by a factor of 100.

of SO₂ to the distance between the instrument and the plume and on the wavelength of the measurement. Figure 1 depicts the model setup schematically and effects influencing the measured absorption signal.

Two different types of model runs were conducted with the radiative transfer model. Type A model runs were set up in an attempt to match the conditions observed during the measurements at Popocatepetl. Afterwards, type B model runs were conducted to examine the differences that might be encountered when flying towards a volcanic cloud of much larger extent, as might be the case after a large-scale volcanic eruption.

For both types of model runs, the ambient atmosphere contained a typical O₃ layer with a maximum concentration of 5×10^{12} molec cm⁻³ at 22 km altitude and total column of 9×10^{18} molec cm⁻² (≈ 330 DU), as this influences the atmospheric radiative transfer in the ultraviolet wavelength region. A 30° solar zenith angle was assumed for the calculations. For all simulations, the instrument was located at the same altitude as the plume centre, and was aimed with a narrow field of view (0.3°) in horizontal direction towards the centre of the plume. Note that both model run types assume a plume which has no concentration gradient from centre to its edges.

3.4.1 Model runs type A: sparsely confined plume with different aerosol contents

In these model runs, the measurement geometry and atmospheric conditions were initialized using the conditions observed during the measurement at Popocatepetl. The volcanic plume was simulated with a centre at 5.5 km altitude, a height of 2 km, a horizontal width of 6.5 km and infinite

Table 3. SO₂ concentrations, AEC and corresponding visibilities of the plume for different type A model runs. For further details see text.

Model run	A1	A2	A3
SO ₂ [10^{12} molec cm ⁻³]	1.54	1.54	0.77
AEC [km^{-1}]	1	10	40
Visibility [m]	4000	400	100

length. All aerosol particles were characterized as purely scattering with a single scattering albedo (SSA) of 1 and a Heyney-Greenstein asymmetry parameter of 0.8, which is typical for scattering sulphate aerosols.

With these boundary conditions, several model runs were performed with variations of the plume's SO₂ concentration and aerosol extinction coefficient (AEC), given in Table 3. For model runs A1 and A2, the SO₂ concentration would result in a measured SCD of 1×10^{18} molec cm⁻² if measured from the edge of the plume without occurrence of multiple scattering. For model run A3 the SO₂ concentration was reduced in order to reproduce column densities similar to those observed in the aircraft measurements.

3.4.2 Model runs B: large scale SO₂ clouds

This scenario has been chosen to model the response of the proposed technique to volcanic clouds, as they might occur after large scale volcanic eruptions. Once the volcanic plume has travelled a large distance from the volcano, its horizontal dimensions are typically such that they considerably exceed the mean free photon path length in the atmosphere (several 10 km). In such cases, light entering a UV-spectroscopic instrument will not have passed through the entire volcanic cloud. To test the sensitivity of such instruments to large scale volcanic SO₂ clouds, model runs B were set up using a SO₂ cloud with infinite extent in one horizontal direction at 10 km altitude. A SO₂ concentration of 1×10^{12} molec cm⁻³ was assumed for the simulation. Aerosol particles are simulated in model run B1 as in model runs A as purely scattering with a SSA of 1, a Heyney-Greenstein asymmetry parameter of 0.8, assuming scattering of sulphate aerosols. The cloud exhibited an AEC of 0.1 km^{-1} . Additionally model run B2 is performed which simulates different ash contents of the cloud. The ash is assumed to have a SSA of 0.8, which can be regarded as a conservative estimation of SSA of ash (Prata and Grant, 2001; Pavlonis et al., 2006; Kudo et al., 2008). The varying ash contents are studied by assuming different AEC of 0.1 km^{-1} , 0.5 km^{-1} , 1 km^{-1} and 4 km^{-1} . The SO₂ concentration is the same as in B1.

The results of this model runs will be discussed in Sect. 5 to give an outlook on the base of the conducted measurements.

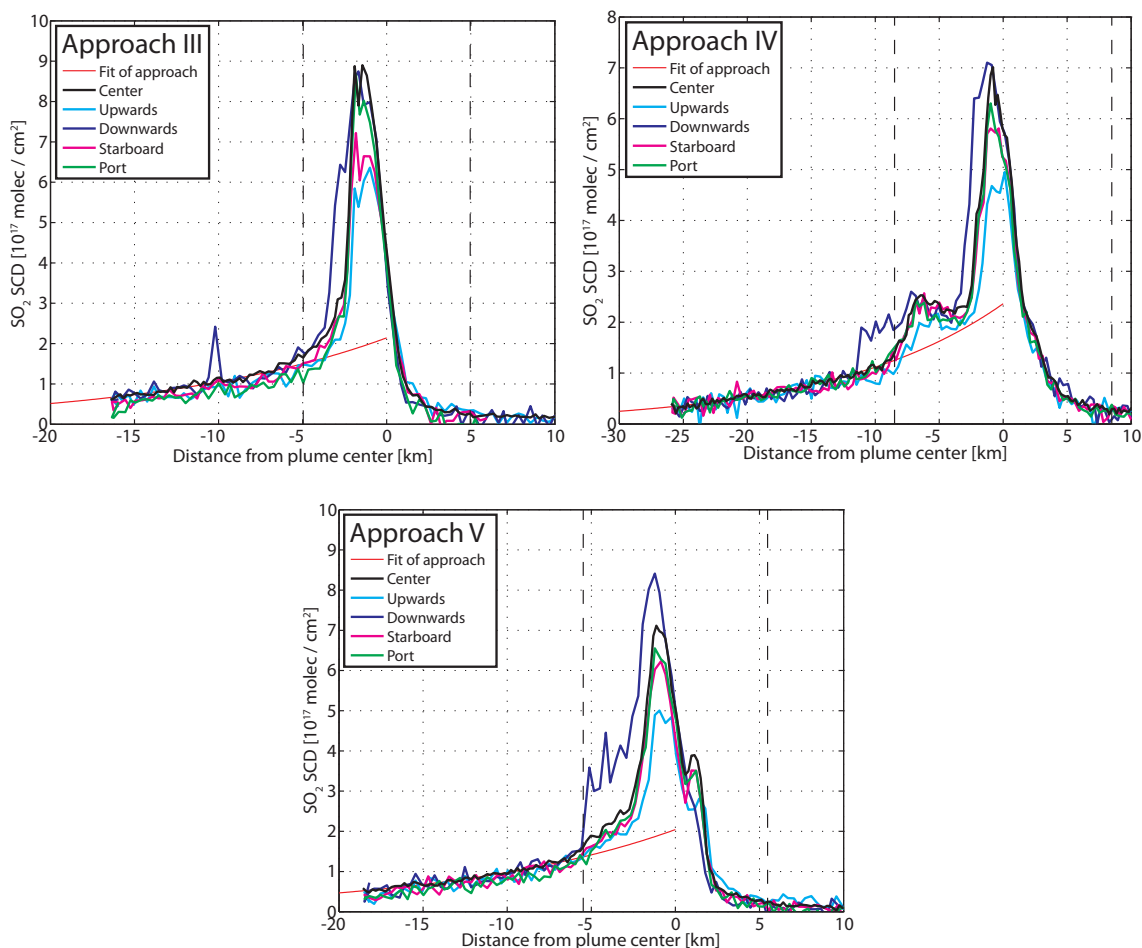


Fig. 6. Results from approaches III–V. The solid red lines indicate the fit of Eq. (2) to the measurement results in the far field. Dashed vertical lines indicate regime C. Errors of measurements are given in Table 1. SO₂ was detected from the first measurements onwards. Significant differences between the retrieved SCDs of the telescopes can not be distinguished for measurements at greater distance to the plume due to the inferior signal-to-noise ratio of the Ocean Optics S2000 spectrometers (up, down, starboard, port viewing directions). Still, a vertical extension of the volcanic plume of at least 2 km can be deduced from the measurements at different vertical directions.

4 Results

4.1 Measurement results from airborne observations

All approaches successfully detected SO₂ from the first measurement of the approaches onwards, but restrictions in airspace prevented measurements at distances further than 25 km from the plume. Figure 6 depicts the SO₂ column densities as a function of distance from the plume centre for approaches III through V for the different viewing directions. The mean error σ for a measurement is specified in Table 1 (see Sect. 3.3). The result of the retrieval for the spectrum gathered at greatest distance to the plume (first spectrum of approach IV) is shown in Fig. 7.

4.1.1 Measurement regimes and extent of plume

First, the SO₂ column time series are discussed. At 25 km distance to the plume, the FOV of each telescope corresponds to a circle of 200 m diameter at the plume, their centre being 2 km apart for the horizontal and vertical off-centred viewing directions, respectively. Thus it can be assumed that the centre, port and starboard looking telescopes started measuring in regime B (plume fills FOV), and the upwards and downwards looking telescopes started at regime B or in the transition from measurement regime A (plume partly fills FOV) to B. Due to the lower signal to noise ratio of the S2000 spectrograph (up, down, port, starboard telescope), a clear transition point can not be distinguished. In order to discuss the transition between regime B and C, the airborne approaches are best compared to ground based car traverses.

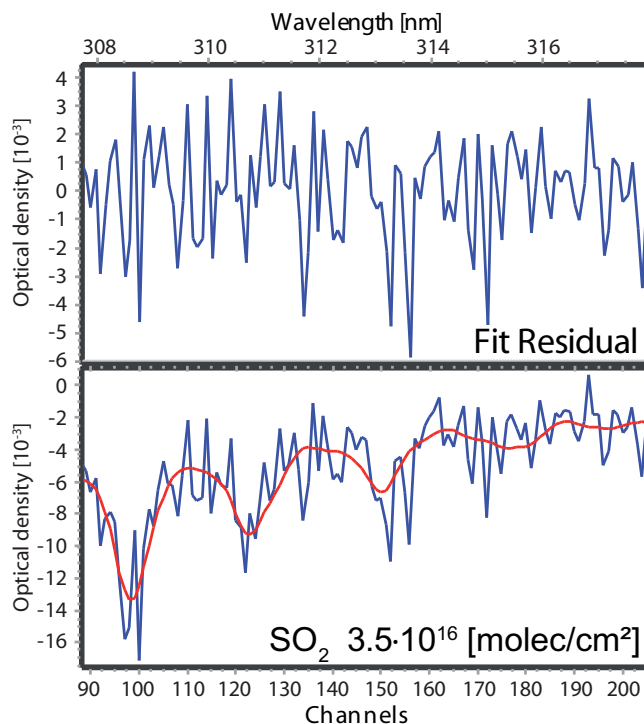


Fig. 7. Fit result for the spectrum gathered at greatest distance (first spectrum of approach IV), taken at 25 km distance. Shown is the residual above and the fitted SO₂ SCD of 3.5×10^{16} molec cm⁻² below.

Approach II was performed approximately between 16:06 h–16:10 h UTC and compared with car traverse 2, which was measured from 15:34 h–16:05 h UTC. It can not be used in the study on SO₂ detectability due to changes in flight altitude in the first minute. However, the plane did not change direction during the rest of approach II and while travelling through the plume. Due to its close proximity to the car traverses in space and time, it can be used to compare both measurements. For that purpose, the ground based measurements were interpolated onto the path of the airplane approach assuming a linear expansion from the source to each measurement point. The result is depicted in Fig. 8. The plume can be well approximated by a gaussian fitted to the car traverses, which sets the plume center at 0 km at the maximum of the gaussian.

Comparing airborne approach II and car traverse 2, the expected characteristics as argued in Sect. 2, Fig. 1, are clearly visible. The SO₂ SCD of the airborne measurements is increasing approximately until entering the plume, which horizontal distribution is captured by the car traverses. It is also apparent, that the maximum SO₂ SCD of the airplane approach does occur almost, but not exactly at the edge of the plume but not exactly at the edge of the plume. It is rather measured several hundred meters inside the plume. It is rather measured several hundred meters inside the plume.

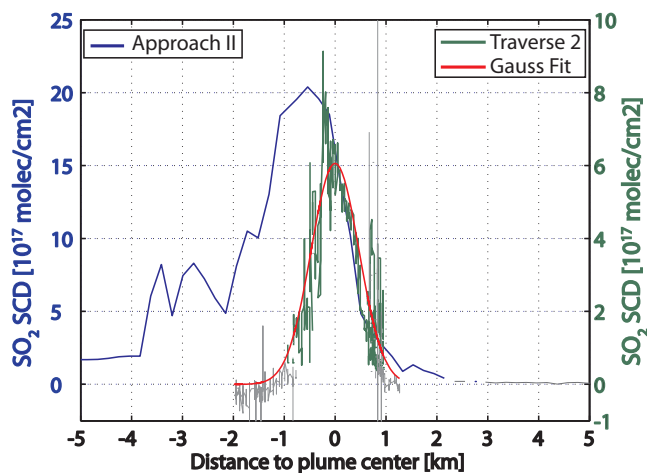


Fig. 8. Comparison of results from car traverses and airborne measurements, with scale of measured SO₂ SCDs on the right and left ordinate, respectively. Values below 3x measurement error are drawn in grey. Strong variations in the car traverse (e.g. at 1 km from plume centre) are artefacts due to vegetation blocking the view. The gradients shown agree with expected characteristics of transition between regime B to regime C (see Fig. 1), although the starting point of the plume of the car traverse does not correlate with the maximum of the values retrieved from the airborne measurement.

The model results discussed in Sect. 4.3 show that the retrieved SO₂ SCDs might change significantly with the transition from outside to inside the plume, with a shift of the maximum SO₂ SCD to the centre of the plume with increasing AEC. Thus the comparison between car traverse and airborne approach indicates that multiple scattering inside the plume causes the maximum column density to be measured within the plume, not at its front edge.

Airborne approaches III–V crossed the plume further downwind. Thus plume position and size can not be simply extrapolated from the ground based measurements to the location of the airborne measurements. Also, the exact plume position can only be approximated from airborne measurements applying only forward looking DOAS telescopes.

The exponential relationship (Eq. 2) between retrieved SCD and distance to source as derived in Appendix A, is only valid in regime B. Also, approximations made might not hold for higher SO₂ SCDs and in close proximity of the plume, in which light scattered into the viewing direction of the telescope might still be affected by absorption structures from the plume's gases. Thus regime C is approximated by fitting function 2 to the signal of the centre looking telescope for the far field of approaches III, IV and V. The start of regime C was set to the start of a steadily increasing difference ($> 2.5 \times 10^{16}$ molec cm⁻²) between fitted curve and retrieved values. The end of the plume is reached when the SO₂ values are below the detection limit of the instrument.

The so determined regime C is marked by the dashed vertical lines in Fig. 6.

4.1.2 Spatial separability of the different viewing directions

The airplane was flying at the same altitude as the volcanic plume and approached it from the side. Although SO₂ was detected by all instruments from the first measurement onwards, significant differences between the retrieved SCDs of the telescopes can not be distinguished for measurements at greater distance to the plume. The signal-to-noise ratio of the Ocean Optics S2000 spectrometers used for the measurements with non-centre-looking telescopes was inferior to that of the QE65000 (centre-looking telescope). Thus the precision of the measurements done with the S2000 was not sufficient to detect differences in SO₂ column at large distances from the plume.

Theoretically, SO₂ SCDs measured in starboard, centre and port direction during the approach should not differ greatly for a homogeneous plume along its path of propagation. For the vertical viewing directions (down, centre, up), differences in signal should depend on the distance to the plume and its vertical extent. At some point close to the edge or inside the plume, the gradients of all instruments should coincide until the plume is passed (and afterwards showing no SO₂ signal), because the different telescopes are observing increasingly similar parts of the plume.

While the plane approaches, the upward and downward looking instruments start observing the plume and their gradients should increase and start converging to the gradient of the centre looking instrument, because the different telescopes are observing increasingly similar parts of the plume. Again, at some point at the edge or inside the plume, the gradients of all instruments should coincide until the plume is passed (and afterwards showing no SO₂ signal).

Comparing the horizontally sideways pointing telescopes, similar SO₂ gradients are observed at most times except for approach III, where a change in flight direction while inside the plume lead to a strong increase in the port signal (see also Fig. 3).

For the different vertical viewing directions, differences in the results obtained become more pronounced when the measurements are performed in and close to regime C. The telescope looking downwards always detects a significantly higher SO₂ SCD than the upwards looking telescope. Furthermore, it shows a comparable (Approach III and IV) or greater (Approach V) SO₂ SCD than the centre looking telescope. Possible issues discussed are (1) the plume was traversed above its centre altitude although results from the ground based measurements indicate that the plume's height was slightly above the plane's approach altitude (see Sect. 4.2). Changes in plume height due to e.g. Lee-waves cannot be ruled out, but as described above, the differences in optical path lengths inside the plume should become neg-

ligible closer to the plume. (2) A severe misalignment of telescopes; this can be ruled out, because even at greatest distances all telescopes observed the plume. (3) Strong small scale inhomogeneities of SO₂ concentrations inside the volcanic plume should be negligible due turbulences between source and measured plume section. (4) light detected by the downward looking telescope is subject to an increased path length inside the plume; this effect is certainly present but should only be of second order, because the telescopes are observing very similar plume cross sections as discussed above. (5) Errors in calibration and instrumental function for the different spectrograph should lead to additional structures in the residuum of the DOAS fit algorithm. This was not observed. A final conclusion is not possible because additional calibration quartz glass cells filled with SO₂ were not available to perform calibration and comparison of the different viewing directions.

Although early detection capabilities of DOAS for SO₂ could be proven, future studies are necessary with higher grade spectrometers for all viewing directions combined with additional calibration and instrument intercomparison. This includes additional modelling to assess radiative transfer effects for the different viewing directions.

4.2 The ground based measurements

The wind direction derived from automobile based measurements (the direction between the volcano's summit and the maximum encountered column densities) are depicted in Fig. 9. Both car traverses and the stationary ground-based instruments yield comparable wind directions with an average of 232° N. The small systematic differences between the results of the two methods might be explained by the different cross sections of the plume seen by each measurement technique. Also, the algorithm for the stationary instruments assumes that both instruments are measuring the same cross section of the plume. Regardless of these small systematic errors, the results clearly show the stability of meteorological conditions during the time of the airborne approaches. The altitude of the centre of the plume was calculated to be between 5250 and 5750 m a.s.l., the spread of plume heights can be explained by varying emission strengths and wind speeds. Stronger winds tend to press the plume slightly downwards in the proximity of the volcano. Given the summit height of 5426 m a.s.l., the retrieved plume heights correspond well to the visual observations of a plume at approximately the same or slightly lower altitude as Popocatepetl's summit.

Comparing the altitude of plume centre derived by the two stationary instruments with the altitude of airplane approaches, the plume's centre is generally measured about 200 m higher than the mean altitude of airplane approaches (5250 m a.s.l.). These measurements confirm that the airplane approaches were performed at the approximate plume height and during stable meteorological conditions.

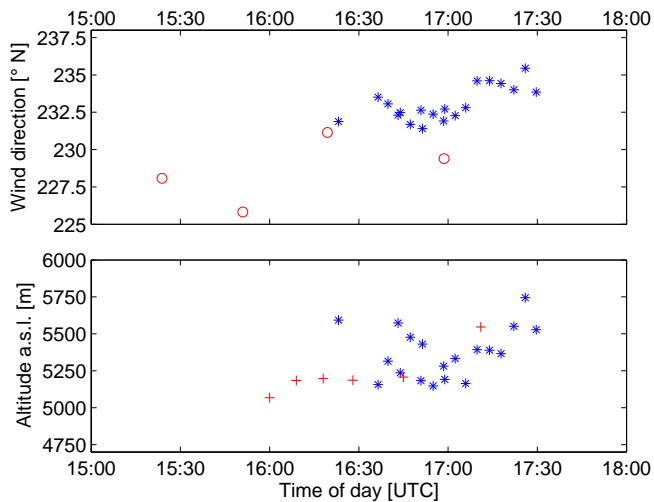


Fig. 9. Wind direction and altitude of plume centre derived from the ground based measurements, showing the stable meteorological conditions on 24 April 2010. Values derived by the two stationary scanning instruments according to (Galle et al., 2010) are depicted as blue asterisks, red circles show results from the car traverses (upper graph). Also the mean altitude of the airplane is indicated for all approaches by red pluses (bottom graph). Note that the different types of measurements were conducted at different distances to the plume, which could explain the slightly differing values.

4.3 Results from radiative transfer study

Here, model runs A will be discussed because they allow conclusions over the measurements. The reader is referred to Sect. 5 for the results of model run type B as an outlook on bases of the conducted experiment. As exemplary result of the model runs A, model run A2 is shown in Fig. 10. Its AEC was chosen, so that the gradients of measurements and model run A2 match qualitatively (see also Fig. 6). With an assumed FOV of 5.2 mrad (0.3°), at the maximum distance modelled (100 km) a circle of diameter of ≈ 520 m is observed at the plume. Thus all modelled approaches correspond to measurements in regime B and C.

In Fig. 10, the dependency of the measured SO₂ SCD on distance can be seen. The gradient of the retrieved SO₂ SCD follows the expected line with a clear separation of wavelengths. Longer wavelengths are less affected by Rayleigh scattering than smaller ones and thus less dependent on distance to the cloud. This leads to a difference in relative decrease of about a factor 10 at 100 km distance to the plume.

Studying the transition between simulated measurements in regime B and regime C (the plume is indicated as a grey shaded area), some interesting features are immediately visible: intuitively, one would suspect the maximum SO₂ signal just when the plane enters the plume, because light can no longer be scattered into the instrument's field of view without having passed the plume. This is reproduced by the model

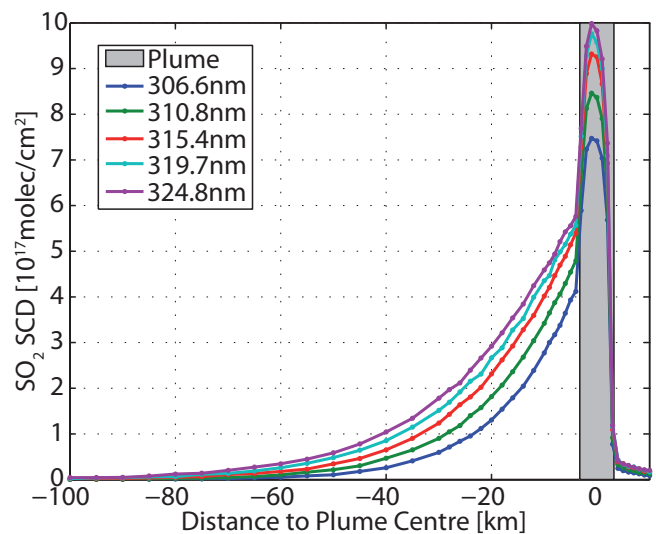


Fig. 10. The figure shows the results of model run A2. The AEC was set to 10 km^{-1} corresponding to a visibility of 400 m inside the plume, which is marked as shaded area. The graph depicts simulated SO₂ column density as a function of the distance of the instrument from the plume.

run A1 when low AEC is assumed. With increasing AEC in model runs A2 and A3 however, a shift to the centre of the plume becomes apparent of maximum SCDs. Also, a sharp edge can be seen in the SCD distribution at the position where the aircraft enters the plume (+3.25 km). This could be the explanation for the distribution observed in the measurement and the differences shown between car traverse and plane approach II (Fig. 8). Measurements taken at the front edge of the plume are not detecting radiation that has penetrated the entire plume, but rather measure light scattered by aerosols in the front portion of the plume. On the other hand, measurements taken inside the plume can be affected by significant enhancement of the light path inside the plume due to multiple scattering. Although the modelled cases are greatly simplified, e.g. a real plume is not evenly distributed over a discrete interval, they show that the maximum SO₂ column is not necessarily detected at the front edge of the plume. Thus, care must be taken when judging which spectra have been taken in and outside of the plume (regime B and C, respectively).

5 Comparing measurements to model results: inferring maximum distance at which SO₂ can be detected

To compare model results and measurements, an exponential function was fit to the different approaches. It is based upon a simplified determination of visibility and contrast that can be found in textbooks about radiation transport in the atmosphere (e.g. Platt and Stutz, 2008, p. 110) and an analogue

Table 4. Results from the fits of function (2) to approaches III–V.

	Approach	III	IV	V	Mean
ϵ	[10 ⁻⁵ m ⁻¹]	7.13	7.50	7.37	7.33
conf ϵ	[10 ⁻⁶ m ⁻¹]	0.81	0.30	0.47	0.53
A	[10 ¹⁷ molec cm ⁻²]	2.14	2.34	2.04	2.18
conf A	[10 ¹⁷ molec cm ⁻²]	0.20	0.10	0.12	0.14
r^2		0.89	0.97	0.95	0.94

has been applied for radiative transfer corrections of UV-camera measurements in Bluth et al. (2007).

$$\frac{S(L_2)}{S(L_1)} \approx e^{-\epsilon \times (L_2 - L_1)} \quad (1)$$

The above function describes the relative change of retrieved SCD $S(L_1)$ and $S(L_2)$ between distance L_1 and L_2 to the plume. For a detailed derivation see Appendix A. ϵ is the total extinction coefficient depending on Rayleigh and Mie scattering, retrieval wavelength range and the distribution of absorption structure of the trace gas of interest in the respective retrieval wavelength range. Because the retrieved SCDs all possess a certain error, it is advantageous to use

$$S(L) = A \times e^{-\epsilon \times L} \quad (2)$$

where A is a hypothetical SCD at zero distance or in our case the plume's centre. Function (2) is only valid for measurements taken in the regime B (see Fig. 1). Also, the “narrow beam” approximation must hold, thus light scattered into the viewing directions should not have passed the plume at an earlier point. In order to ensure these boundary conditions, only measurements taken more than 8 km from the assumed plume centre were used to retrieve the parameters of function (2) for the respective approaches.

The results for all fits are depicted in Fig. 11. They are extrapolated to 50 km distance to the plume. The individual obtained parameters are also shown in Table 4. The mean extinction coefficient ϵ returned by the fit was $7.33 \times 10^{-5} \text{ m}^{-1}$, and the mean coefficient of determination r^2 was 0.94. Thus with the experimental setup, which was not specially tuned for this kind of measurements, and a detection limit of $1.6 \times 10^{16} \text{ molec cm}^{-2}$ for the centre looking telescope (Table 1), the plume of Popocatepetl could have been detected from a distance greater than 35 km.

In order to compare the measurements to the modelled results, function 2 was fitted also to all model runs type A. The fit was performed between 10 and 100 km. The model runs are reproduced well by the analytical approach. All fits achieve a coefficient of determination (r^2) of more than 99.8 %. Table 5 summarizes the fitted extinction coefficients ϵ for 306.6 nm and 310.8 nm of model runs A1, A2 and A3. For model run A1 the fitted extinction coefficient is slightly increased in comparison to the other two. The reason is that

Table 5. Results from the fits to the radiative transfer models. ϵ and the $\pm\Delta$ to calculate confidence bands of 95 % (conf ϵ) are given in [10⁻⁵ m⁻¹].

Modell run		A1	A2	A3	Mean
306.6 nm	ϵ	9.08	7.63	7.14	7.95
	conf ϵ	0.166	0.089	0.136	0.130
	r^2	0.9994	0.9998	0.9994	0.9995
310.8 nm	ϵ	7.80	6.65	6.24	6.89
	conf ϵ	0.083	0.105	0.144	0.111
	r^2	0.9998	0.9996	0.9991	0.9995

model run A1 displays stronger absorptions at 10 km distance than the other two model runs. The approximation made in deriving function 2 are only valid for small absorptions and thus for model run A1 an additional systematic error is induced.

The extinction coefficients from the airborne approaches can be compared to the mean extinction coefficients obtained from the model runs. The relative decreases in SCDs calculated from the extinction coefficients of the approaches are encompassed between the mean results obtained for model runs A for 306.6 nm and 310.8 nm. The fitted ϵ of all approaches and their 95 % confidence bands are depicted together with the mean ϵ derived from the model runs A in Fig. 12. The differences between model and measurements can be explained by the wavelength interval used in the DOAS evaluation. The first and strongest absorption line in the DOAS retrieval interval 307.4–317.8 nm is the absorption maximum at 308.7 nm, influencing the DOAS retrieval heavily. Thus, it is consistent that the value of the extinction coefficient ϵ of the DOAS retrieval lies about halfway between the extinction coefficients of 306.6 nm and 310.8 nm of the modelled scenarios. These results validate the model runs and allow to extent the experimental “proof of concept” measurement with model run B.

Early detection of an extensive volcanic cloud, results model runs B

As an example for the response of the proposed early detection system, an extensive volcanic cloud was simulated in model runs type B. The volcanic cloud was modelled with infinite horizontal extent and was located at 10 km altitude, a typical flight altitude for commercial airplanes. The results of model run B1 are shown in Fig. 13. A cloud containing mainly sulfate aerosols is assumed. Note that in contrast to Fig. 10, the ordinate is displaying a logarithmic scale to enhance visibility of the gradients at large distances to the volcanic cloud. Again, a clear separation of retrieved SO₂ SCDs at different wavelength intervals with distance can be observed.

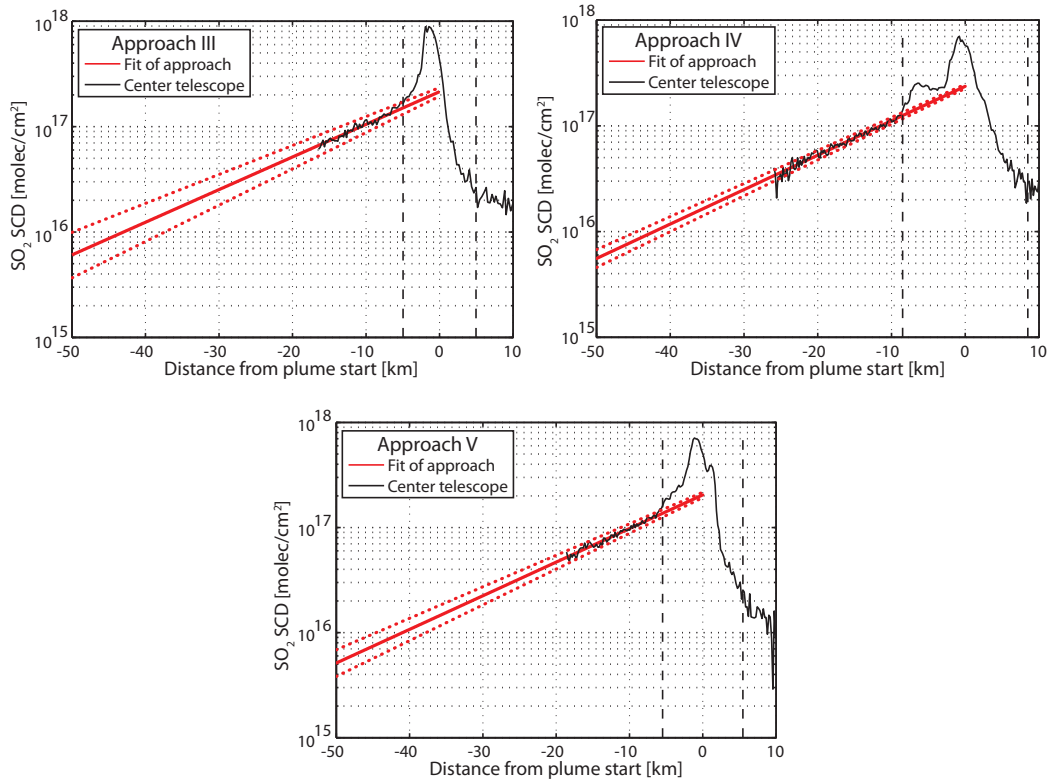


Fig. 11. Approaches III–V extrapolated to 50 km distance. Fitted function is depicted as red line with 95 % confidence bands as red dots. Measurement regime C is indicated by dashed vertical lines.

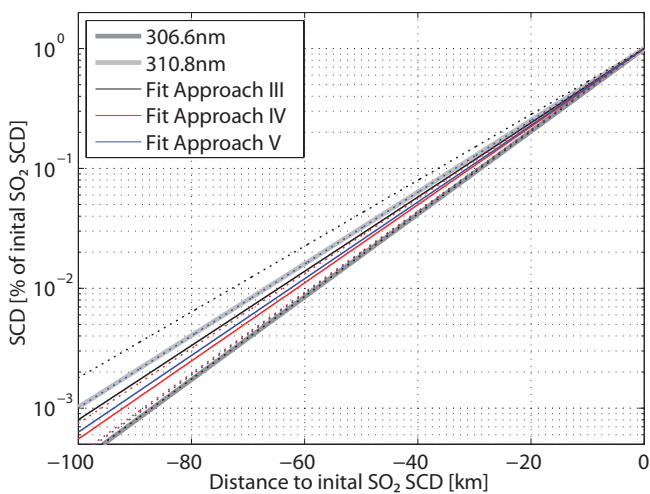


Fig. 12. Relative changes of SO₂ SCDs for approaches III–V and comparison to the mean extinction coefficients derived by model runs A1–A3. The dashed lines indicate the 95 % confidence interval.

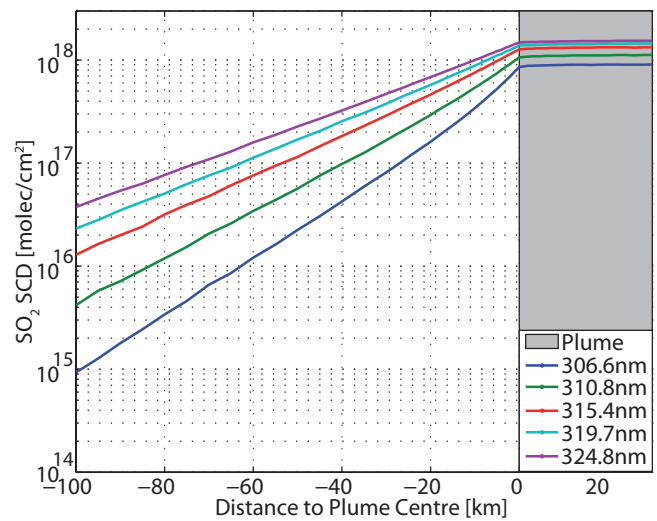


Fig. 13. Simulated SO₂ SCD from model scenario B1. Here, a volcanic cloud with infinite extent in propagation direction and from the edge onwards was assumed to be at 10 km altitude. An SO₂ concentration of 1×10^{12} molec cm⁻³ is assumed for the simulation, and the cloud exhibited an aerosol optical depth of 0.1 km⁻¹.

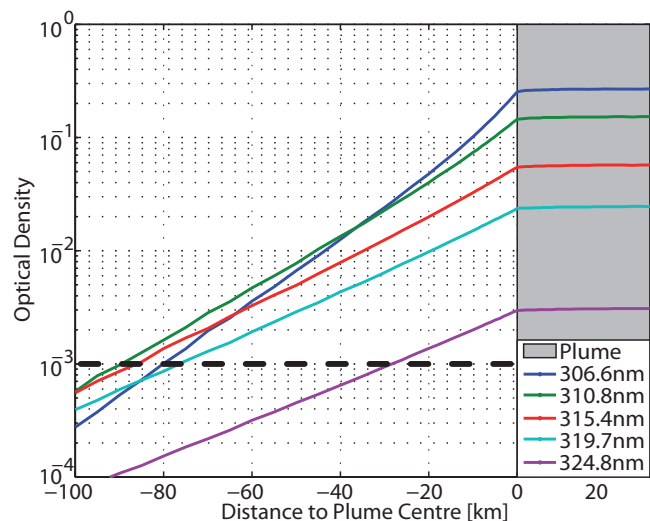


Fig. 14. Optical densities are shown for model scenario B1 in order to assess detectability of large scale volcanic cloud. Optical densities of more than 10^{-3} are still obtained at distances greater than 80 km from the plume for the wavelength range 310–315 nm, thus indicating the possibility of a significantly earlier detection than is possible at lower altitudes.

The relative changes in signal strength do not directly correspond to relative changes in detectability because the SO₂ absorption cross-section decreases with wavelength. The detection limit is instead given by the optical density obtained in a measurement, which is the product of the column density and the differential absorption cross-section. For model run B1, the simulated optical density is depicted as a function of wavelength in Fig. 14. A typical DOAS instrument which has been tuned to the task might be able to resolve optical densities of about 10^{-3} at a measurement integration time of a few seconds. This limit is reached at 80–90 km distance to the volcanic cloud for the wavelength range 310–315 nm. Thus, given a slightly enhanced setup, there is a realistic option of a feasible early detection of a volcanic SO₂ cloud at these distances.

The results of model run B2 show the systems response to varying ash contents of the volcanic cloud. Ash was simulated by decreasing the single scatter albedo (SSA) of the plume aerosol to 0.8. This is thought to represent a lower limit for the SSA of an ash-rich volcanic cloud (see e.g. Prata and Grant, 2001; Pavolonis et al., 2006; Kudo et al., 2008). The modelled optical densities obtained for 310.8 nm are shown in Fig. 15, as the highest sensitivity was obtained at this wavelength for model run B1. For comparison, the result of B1 (Fig. 14) for 310.8 nm is depicted as a dashed blue line. Reducing the SSA from 1 to 0.8 at an aerosol extinction coefficient (AEC) of 0.1 km^{-1} reduces the sensitivity very slightly, decreasing the detection range from about 90 km to 85 km. However, a further reduction in signal is observed

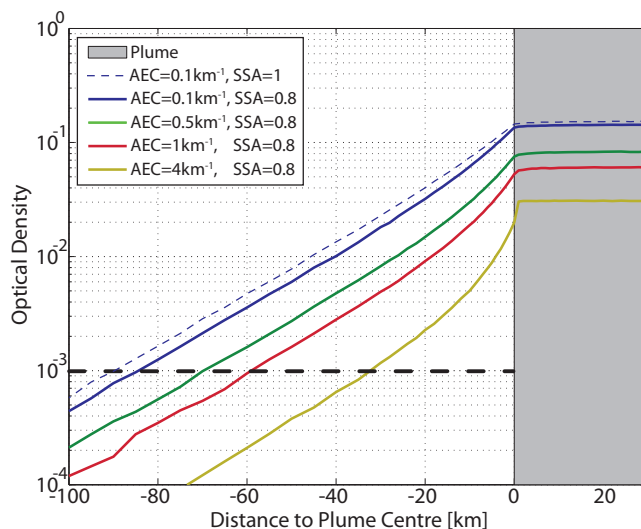


Fig. 15. Optical densities for model scenario B2: Depicted are Simulated Optical densities at 310.8 nm as a function of distance to an extended volcanic cloud (scenario B2) and varying ash content. Volcanic ash is simulated with a SSA=0.8 and varying AECs. For comparison, the dashed blue line shows the result for a cloud with a purely scattering aerosols at an AEC of 0.1 km^{-1} (see Fig. 14). The dashed black line represents the assumed detection limit of 10^{-3} in optical density. Higher ash content reduces the detection limit, but a detection range of $> 60 \text{ km}$ is still obtained for $\text{AEC} < 1$. Only for extremely thick plumes, such as those encountered in close proximity to the volcanic source, does the detection range drop further.

for optically thick plumes, as the light path inside the cloud is reduced. Moderate AECs of $< 1 \text{ km}^{-1}$ lead to a decrease of the maximum distance of detection from $> 80 \text{ km}$ to about 60 km. A very thick cloud with an AEC of 4 km^{-1} would only be detectable from $\approx 35 \text{ km}$ distance. However, such a cloud would be clearly visible in the sky, as the scattering extinction length is only 250 m. While such conditions may be encountered in close proximity to the volcanic source, they are not typical of a large-scale, diluted volcanic cloud that has travelled many tens or hundreds of kilometres in the atmosphere.

6 Conclusions

The measurements presented here clearly demonstrate the general applicability of DOAS as an early detection technique for SO₂ in a “proof of concept” campaign. A number of plume approaches were flown, and the measurement results were reproduced with a radiative transfer model. Although the approaches were only started at up to 25 km distance to the plume, the found relationship of signal to distance of the measurements could be used to extrapolate the experiment to 100 km distance. Due to the lower air pressure at typical flight altitudes (about 10 km) when compared

to the altitude of the Popocatepetl plume, additional radiative transfer studies conclude that a volcanic plume with a SO₂ slant column density of 10¹⁸ molecules cm⁻² as viewed from the outside can be detected at distances up to 80 km away for both, a cloud consisting only of purely scattering sulfate aerosols (SSA = 1) and a cloud consisting of ash with a SSA of 0.8. This range provides enough time for pilots to take actions to avoid plume fly-through under typical flight conditions, suggesting that this technique can be used as an effective aid to prevent dangerous aircraft encounters with potentially ash-laden volcanic plumes.

However, certain issues must be addressed. Because the technique is based on radiation in the UV spectral region, it is only applicable during daylight. At twilight the signal to noise ratio will drop due to reduced intensities in the UV, which can partly be compensated by longer exposure times with consequent lower measurement frequency. The technique does not detect the main hazard volcanic ash. Although certain algorithms have been proposed which should be able to determine aerosol optical densities of the plume from UV measurements (Kern et al., 2010b), these concepts need high computational power and are not feasible for real time evaluation. SO₂ is only a good proxy for ash which is the greater hazard if there is no separation of the ash and SO₂ cloud. Thus the technique is only complementary to ash detection systems in the IR.

One has to keep in mind that this study is only “proof of concept” and does not present a mature system. Further efforts are needed in experiment and modelling to fully explore the capabilities of the technique. This includes the ability to spatially resolve volcanic plumes at greater distances in order to allow avoidance measures to be initiated. Strategies must be developed to supply clear sky reference spectra without SO₂ absorptions. One approach would be to construct a small database with reference spectra constructed from high resolution solar spectra (e.g. Chance and Kurucz, 2010) including dependencies on altitude, solar zenith and azimuth angle. Furthermore, algorithms need to be developed which reduce or eliminate the influence of a SO₂ cloud above or below the aircraft which could influence the perceived signal at all viewing directions. Also investigations of the limitations e.g. in case of high altitude clouds between plume and instrument need to be done. This includes sensitivity to a volcanic cloud with ash particles covered in ice, because this is one of the cases where IR techniques based on the reverse absorption method are not suitable.

Last but not least, great potential lies in the development of DOAS instruments developed to this specific task. Large volcanic clouds are much more easily evaded by flying over or under them than by trying to go around them. Therefore, the vertical direction is arguably more important than the horizontal one. E.g. one could imagine a DOAS instrument applying an imaging spectrometer, which could be positioned so that its spatial axis is in the vertical, its dispersive axis is horizontal (IDOAS, Louban et al., 2009).

Besides the limitations and need for future research mentioned above, DOAS based SO₂ detection is a complementary technique to the detection of ash in the infra-red regime and in combination can greatly mitigate the risk from volcanic clouds to aviation.

Appendix A

Analytical approach to the radiation dilution effect

In general, the propagation of radiation in the atmosphere is a complex process. Multiple scattering inside and light dilution outside the plume both affect the measured signal. For a valid assessment of volcanic emissions both effects need to be taken into account. For this study, the gradient of measured SO₂ SCDs with distance between instrument and plume needs to be determined to assess the feasibility of DOAS as an early detection system for SO₂. The true concentrations inside the plume are only of secondary concern, and we focus on radiation dilution.

An analytical solution can be derived to estimate the dependency of measured SCD to distance to the volcanic plume. The approach is analogous to the simplified determination of visibility and contrast that can be found in text books about radiation transport in the atmosphere (e.g. Platt and Stutz, 2008, p. 110). A similar strategy has been applied for radiative transfer corrections of UV-camera measurements in Bluth et al. (2007).

There, a black object of zero intensity is viewed from distance L with a background intensity I_0 next to the object. Radiation scattered into the field of view of the observer will lead to an increase of the perceived intensity I_R with increasing distance to the object until background intensity I_0 is reached. Certain approximations are made. (1) The probability is negligible that a photon is scattered into the viewing direction of the telescope after having been scattered out of it (Narrow Beam approximation). Consequently, extinction, which is comprised as the sum of Rayleigh and Mie scattering, can be treated like absorption as described by Lambert-Beer's Law. In our case it is the radiation scattered into the viewing direction. (2) The atmosphere is considered homogeneous. With these approximations, the scattered radiation intensity I_R received by the observer when looking at a black object at distance L is given by

$$I_R(\lambda) = I_0(\lambda) \times \left(1 - e^{-\epsilon(\lambda) \times L}\right) \quad (\text{A1})$$

where the extinction coefficient $\epsilon(\lambda) = \epsilon_R(\lambda) + \epsilon_M(\lambda)$ is the sum of the Rayleigh and Mie extinction coefficients.

The wavelength dependency of Rayleigh and Mie scattering can be disregarded for a 1st order approximation of the dependency of DOAS retrieval on radiation dilution. Rayleigh scattering is approximately proportional to λ^{-4} , whereas Mie scattering has a wavelength dependency proportional to $\lambda^{-1.3}$. This results in a relative difference of

scattered intensity of $\approx 18\%$ between 10 nm (wavelength range of DOAS retrievals) in the range of 300 nm and 330 nm. The evaluation of SO₂ is strongly dependent on the stronger differential optical absorption features at smaller wavelengths (see Fig. 5). The difference between minima of the differential optical absorption cross sections of SO₂ is (≈ 2 nm). On this scale, the relative difference due to Rayleigh and Mie scattering is only $\approx 3\%$. Thus the error introduced by neglecting the wavelength dependency of Rayleigh and Mie scattering will be at the lower end of the interval 3%–18%.

Measured SO₂ SCDs (S) are proportional to the amplitude of its differential optical absorption structures:

$$S \propto \ln\left(\frac{I_0}{I}\right) \quad (\text{A2})$$

Taking the intensity of absorption minima as background intensity I_0 and absorption maxima as intensity I , a retrieved SO₂ SCD $S(L')$ will decrease with distance to the source. I_1 and I_2 are denoting the intensity at absorption maxima at L_1 and L_2 distance. Applying Eq. (A1), the intensity I_2 can be described in terms of I_1 :

$$\begin{aligned} I_2 &= I_0 \times (1 - e^{-\epsilon \cdot L_2}) \\ &= I_1 + (I_0 - I_1) (1 - e^{-\epsilon \times \Delta L}) \end{aligned} \quad (\text{A3})$$

where ΔL is the difference between L_1 and L_2 . Thus $S(L_2)$ can be written as

$$\begin{aligned} \ln\left(\frac{I_0}{I_2}\right) &= \ln\left(\frac{I_0}{I_1 + (I_0 - I_1) (1 - e^{-\epsilon \times \Delta L})}\right) \\ &= \ln\left(\frac{I_0}{I_0 + (I_1 - I_0) \times e^{-\epsilon \times \Delta L}}\right) \\ &= -\ln\left(\frac{I_0 + (I_1 - I_0) \times e^{-\epsilon \times \Delta L}}{I_0}\right) \\ &= -\ln\left(1 + \frac{I_1 - I_0}{I_0} \times e^{-\epsilon \times \Delta L}\right) \end{aligned} \quad (\text{A4})$$

The logarithm $\ln(\xi)$ can be expressed as a Taylor series if $-1 < \xi < 1$ with

$$\ln(\xi + 1) = \sum_{k=1}^{\infty} (-1)^{k-1} \times \frac{\xi^k}{k} \quad (\text{A5})$$

If ξ is close to 0, the logarithm can be approximated by using only the first term ($\ln(\xi + 1) = \xi$). This means that Eq. (A4) can be estimated by

$$S(L_1) \propto -\frac{I_1 - I_0}{I_0} \quad (\text{A6})$$

$$S(L_2) \propto -\frac{I_1 - I_0}{I_0} \times e^{-\epsilon \times \Delta L} \quad (\text{A7})$$

as long as $I_0 \approx I_1$, which is the case for weak absorber with optical densities on the order of a few percent. The relative

change of SCD $S(L_1)$ to $S(L_2)$ with distance ΔL is given by

$$\begin{aligned} \frac{S(L_2)}{S(L_1)} &= \frac{\ln\left(\frac{I_0}{I_2}\right)}{\ln\left(\frac{I_0}{I_1}\right)} \\ &\approx \frac{\frac{I_1 - I_0}{I_0} \times e^{-\epsilon \times \Delta L}}{\frac{I_1 - I_0}{I_0}} \\ &\approx e^{-\epsilon \times \Delta L} \end{aligned} \quad (\text{A8})$$

Thus Eq. (A8) can be used to estimate the dependence of DOAS measurements of a confined trace gas on distance between instrument and absorber. ϵ is an extinction coefficient, which depends on retrieval wavelength range and the absorption structure of the trace gas of interest in the respective retrieval wavelength range. E.g. depending on how the dominant absorption bands of the trace gas of interest are distributed within the retrieval wavelength range. Also, it must be stressed that above approximation is only valid for weak absorbers, because all but the first term of Eq. (A5) are omitted.

Acknowledgements. The authors would like to thank the Mexican students who honorary helped with the ground based instruments. Also we would like to thank R. Champion and an anonymous referee for comments and improving the manuscript. The measurements were performed in the frame of the FIEL-Volcan project, funded by the ‘‘Fondo de Cooperaci3n Internacional de Ciencia y Tecnolog3a Uni3n Europea M3xico’’ (FONCICYT, CONACYT-EU) grant 93645.

Edited by: F. Prata

References

- Ash Dispersal Forecast and Civil Aviation Workshop, Consensual Document, Geneva, Switzerland, 2010.
- Barton, I. J. and Prata, A. J.: Detection and discrimination of volcanic ash clouds by infrared radiometry – II: experimental. Casadevall, T. J. Volcanic Ash and aviation safety: proceedings of the first International Symposium on Volcanic Ash and Aviation Safety, 313–317, US Geological Survey bulletin, 1994.
- Berglen, T. F., Berntsen, T. K., Isaksen, I. S. A., and Sundet, J. K.: A global model of the coupled sulfur/oxidant chemistry in the troposphere: The sulfur cycle, *J. Geophys. Res.*, 109, D19310, doi:10.1029/2003JD003948, 2004.
- Bernard, A. and Rose, W. I.: The injection of sulfuric acid aerosols in the stratosphere by El Chich3n volcano and its related hazards to the international air traffic, *Nat. Hazards*, 3, 59–67, 1990.
- Bluth, G. J. S., Shannon, J. M., Watson, I. M., Prata, A. J., and Realmuto, V. J.: Development of an ultra-violet digital camera for volcanic SO₂ imaging, *J. Volcanol. Geoth. Res.*, 161, 47–56, doi:10.1016/j.jvolgeores.2006.11.004, 2007.
- Bogumil, K., Orphal, J., Homann, T., Voigt, S., Spietz, P., Fleischmann, O., Vogel, A., Hartmann, M., Kromminga, H., Bovensmann, H., Frerick, J., and Burrows, J.: Measurements of molecular absorption spectra with the SCIAMACHY pre-flight model:

- instrument characterization and reference data for atmospheric remote-sensing in the 230–2380 nm region, *J. Photoch. Photobi. A*, 157, 167–184, doi:10.1016/S1010-6030(03)00062-5, 2003.
- Carn, S. A., Krueger, A. J., Krotkov, N. A., Yang, K., and Evans, K.: Tracking volcanic sulfur dioxide clouds for aviation hazard mitigation, *Nat. Hazards*, 51, 325–343, doi:10.1007/s11069-008-9228-4, 2009.
- Casadevall, T.: The 1989–1990 eruption of Redoubt volcano, Alaska – Impact on aircraft operations, *J. Volcanol. Geoth. Res.*, 62, 301–316, 1994.
- Chance, K. and Kurucz, R. L.: An improved high-resolution solar reference spectrum for earth's atmosphere measurements in the ultraviolet, visible, and near infrared. *J. Quant. Spectrosc. Radiat. Transfer*, 111, 1289–1295, doi:10.1016/j.jqsrt.2010.01.036, 2010.
- Clarisse, L., Prata, F., Lacour, J.-L., Hurtmans, D., Clerbaux, C., and Coheur, P.-F.: A correlation method for volcanic ash detection using hyperspectral infrared measurements, *Geophys. Res. Lett.*, 37, L19806, doi:10.1029/2010GL044828, 2010.
- Dalton, M. P., Watson, I. M., Nadeau, P. A., Werner, C., Morrow, W., and Shannon, J. M.: Assessment of the UV camera sulfur dioxide retrieval for point source plumes, *J. Volcanol. Geoth. Res.*, 188, 358–366, doi:10.1016/j.jvolgeores.2009.09.013, 2009.
- Deutschmann, T.: Atmospheric radiative transfer modelling using Monte Carlo methods, Master's thesis, University Heidelberg, 2008.
- Deutschmann, T., Beirle, S., Friess, U., Grzegorski, M., Kern, C., Kritten, L., Platt, U., Prados-Roman, C., Pukite, J., Wagner, T., Werner, B., and Pfeilsticker, K.: The Monte Carlo atmospheric radiative transfer model McArtim: Introduction and validation of Jacobians and 3D features, *J. Quant. Spectrosc. Ra.*, 112, 1119–1137, doi:10.1016/j.jqsrt.2010.12.009, 2011.
- Doasis: DOAS Intelligent System, Institute of Environmental Physics, University Heidelberg, Germany, Version 3.2.3799.23257, <http://www.iup.uni-heidelberg.de/institut/forschung/groups/atmosphere/software>, 2010.
- Doran, J., Abbott, S., Archuleta, J., Bian, X., Chow, J., Coulter, R., de Wekker, S., Edgerton, S., Elliott, S., Fernandez, A., Fast, J., Hubbe, J., King, C., Langley, D., Leach, J., Lee, J., Martin, T., Martinez, D., Martinez, J., Mercado, G., Mora, V., Mulhearn, M., Pena, J., Petty, R., Porch, W., Russell, C., Salas, R., Shannon, J., Shaw, W., Sosa, G., Tellier, L., Templeman, B., Watson, J., White, R., Whiteman, C., and Wolfe, D.: The IMADA-AVER boundary layer experiment in the Mexico City area, *B. Am. Meteorol. Soc.*, 79, 2497–2508, 1998.
- Galle, B., Johansson, M., Rivera, C., Zhang, Y., Kihlman, M., Kern, C., Lehmann, T., Platt, U., Arellano, S., and Hidalgo, S.: Network for Observation of Volcanic and Atmospheric Change (NOVAC) – A global network for volcanic gas monitoring: Network layout and instrument description, *J. Geophys. Res.-Atmos.*, 115, D05304, doi:10.1029/2009JD011823, 2010.
- Grindle, T. and Burcham, F.: Engine Damage to a NASA DC-8-72 Airplane From a High-Altitude Encounter With a Diffuse Volcanic Ash Cloud, Tech. rep., NASA, Dryden Flight Research Center, http://ntrs.nasa.gov/archive/nasa/casi.ntrs.nasa.gov/20030068344_2003079762.pdf, 2003.
- Guffanti, M., Schneider, D. J., Wallace, K. L., Hall, T., Bensimon, D. R., and Salinas, L. S.: Aviation response to a widely dispersed volcanic ash and gas cloud from the August 2008 eruption of Kasatochi, Alaska, USA, *J. Geophys. Res.*, 115, D00L19, doi:10.1029/2010JD013868, 2010.
- Heue, K.-P., Brenninkmeijer, C. A. M., Baker, A. K., Rauthe-Schöch, A., Walter, D., Wagner, T., Hörmann, C., Sihler, H., Dix, B., Frie, U., Platt, U., Martinsson, B. G., van Velthoven, P. F. J., Zahn, A., and Ebinghaus, R.: SO₂ and BrO observation in the plume of the Eyjafjallajökull volcano 2010: CARIBIC and GOME-2 retrievals, *Atmos. Chem. Phys.*, 11, 2973–2989, doi:10.5194/acp-11-2973-2011, 2011.
- ICAO: Manual on Volcanic Ash, Radioactive Material, and Toxic Chemical Clouds, 2nd Edition, International Civil Aviation Organization, 2 Edn., <http://www.paris.icao.int/news/pdf/9691.pdf>, doc 9691-AN/954, 2007.
- Johansson, M., Galle, B., Zhang, Y., Rivera, C., Chen, D., and Wyser, K.: The dual-beam mini-DOAS technique-measurements of volcanic gas emission, plume height and plume speed with a single instrument, *B. Volcanol.*, 71, 747–751, doi:10.1007/s00445-008-0260-8, 2009.
- Kantzas, E. P., McGonigle, A. J. S., Tamburello, G., Aiuppa, A., and Bryant, R. G.: Protocols for UV camera volcanic SO₂ measurements, *J. VOLCANOL. Geoth. Res.*, 194, 55–60, doi:10.1016/j.jvolgeores.2010.05.003, 2010.
- Karagulian, F., Clarisse, L., Clerbaux, C., Prata, A. J., Hurtmans, D., and Coheur, P. F.: Detection of volcanic SO₂, ash, and H₂SO₄ using the Infrared Atmospheric Sounding Interferometer (IASI), *J. Geophys. Res.-Atmos.*, 115, D00L02, doi:10.1029/2009JD012786, 2010.
- Kern, C., Kick, F., Lübcke, P., Vogel, L., Wöhrbach, M., and Platt, U.: Theoretical description of functionality, applications, and limitations of SO₂ cameras for the remote sensing of volcanic plumes, *Atmos. Meas. Tech.*, 3, 733–749, doi:10.5194/amt-3-733-2010, 2010a.
- Kern, C., Deutschmann, T., Vogel, L., Woehrbach, M., Wagner, T., and Platt, U.: Radiative transfer corrections for accurate spectroscopic measurements of volcanic gas emissions, *B. Volcanol.*, 72, 233–247, doi:10.1007/s00445-009-0313-7, 2010b.
- Khokhar, M., Frankenberg, C., Van Roozendaal, M., Beirle, S., Kuhl, S., Richter, A., Platt, U., and Wagner, T.: Satellite observations of atmospheric SO₂ from volcanic eruptions during the time-period of 1996–2002, in: atmospheric remote sensing: earth's surface, troposphere, stratosphere and mesosphere – I, edited by: Burrows, J. P. and Eichmann, K. U., vol. 36 of Advances in space research, 879–887, Elsevier Science LTD, The Boulevard, Langford Lane, Kidlington, Oxford OX5 1GB, Oxon, UK, doi:10.1016/j.asr.2005.04.114, 2005.
- Khokhar, M. F., Platt, U., and Wagner, T.: Temporal trends of anthropogenic SO₂ emitted by non-ferrous metal smelters in Peru and Russia estimated from Satellite observations, *Atmos. Chem. Phys. Discuss.*, 8, 17393–17422, doi:10.5194/acpd-8-17393-2008, 2008.
- Kraus, S. G.: DOASIS, A Framework Design for DOAS, Ph.D. thesis, University of Mannheim, 2006.
- Krueger, A.: Sighting of El Chichón sulfur dioxide clouds with the Nimbus 7 total ozone mapping spectrometer, *Science*, 220, 1377–1379, 1983.
- Kudo R., Uchiyama A., Yamazaki A., Kobayashi E. and Nishizawa T.: Retrieval of aerosol single-scattering properties from diffuse and direct irradiances: Numerical studies, *J. Geophys. Res.*, 113,

- D09204, doi:10.1029/2007JD009239, 2008.
- Kurucz, R. L.: High resolution irradiance spectrum from 300 to 1000 nm, AFRL Transmission Meeting, Lexington, Mass, <http://kurucz.harvard.edu/sun.html>, 2005.
- Lehmann, T.: Improving the sensitivity of spectroscopic measurements of atmospheric trace gases by modern signal processing algorithms, Ph.D. thesis, IUP, University Heidelberg, in preparation, 2011.
- Louban, I., Bobrowski, N., Rouwet, D., Inguaggiato, S., and Platt, U.: Imaging DOAS for volcanological applications, *B. Volcanol.*, 71, 753–765, doi:10.1007/s00445-008-0262-6, 2009.
- Lübcke, P.: Development of a new SO₂ camera for volcanic gas flux measurements, Master's thesis, Institute of Environmental Science, University Heidelberg, 2010.
- Miller, T. and Casadevall, T.: Encyclopedia of volcanoes, chap. Volcanic ash hazards to aviation, Academic Press, San Diego, USA, 2000.
- Mori, T. and Burton, M.: The SO₂ camera: A simple, fast and cheap method for ground-based imaging of SO₂ in volcanic plumes, *Geophys. Res. Lett.*, 33, L24804, doi:10.1029/2006GL027916, 2006.
- Mori, T., Mori, T., Kazahaya, K., Ohwada, M., Hirabayashi, J., and Yoshikawa, S.: Effect of UV scattering on SO₂ emission rate measurements, *Geophys. Res. Lett.*, 33, L17315, doi:10.1029/2006GL026285, 2006.
- Pavolonis, M. and Sieglaff, J.: GOES-R Advanced Baseline Imager (ABI) Algorithm Theoretical Basis Document For Volcanic Ash (Detection and Height), Tech. rep., STAR, NESDIS, NOAA, Camp Springs, Maryland, USA, http://www.goes-r.gov/products/ATBDs/baseline/Aviation_VolAsh_v2.0.no.color.pdf, 2010.
- Pavolonis, M. J., Feltz, W. F., Heidinger, A. K., and Gallina, G. M.: A daytime complement to the reverse absorption technique for improved automated detection of volcanic ash, *J. Atmos. Ocean. Tech.*, 23, 1422–1444, 2006.
- Platt, U. and Stutz, J.: Differential Optical Absorption Spectroscopy: Principles and Application, Springer, doi:10.1007/978-3-540-75776-4, 2008.
- Prata, A.: Infrared radiative-transfer calculations for volcanic ash clouds, *Geophys. Res. Lett.*, 16, 1293–1296, 1989.
- Prata, A. J.: Satellite detection of hazardous volcanic clouds and the risk to global air traffic, *Nat. Hazards*, 51, 303–324, doi:10.1007/s11069-008-9273-z, 2009.
- Prata, A. J. and Bernardo, C.: Retrieval of volcanic SO₂ column abundance from atmospheric infrared sounder data, *J. Geophys. Res.-Atmos.*, 112, D20204, doi:10.1029/2006JD007955, 2007.
- Prata, A. J. and Bernardo, C.: Retrieval of volcanic ash particle size, mass and optical depth from a ground-based thermal infrared camera, *J. Volcanol. Geoth. Res.*, 186, 91–107, doi:10.1016/j.jvolgeores.2009.02.007, 2009.
- Prata, A. J. and Grant, I. F.: Retrieval of microphysical and morphological properties of volcanic ash plumes from satellite data: Application to Mt Ruapehu, New Zealand. *Q. J. Roy. Meteor. Soc.*, 127, 2153–2179, doi:10.1256/smsqj.57614, 2001.
- Prata, A. J. and Tupper, A.: Aviation hazards from volcanoes: the state of the science, *Nat. Hazards*, 51, 239–244, doi:10.1007/s11069-009-9415-y, 2009.
- Prata, A., Barton, I., Johnson, R., Kamo, K., and Kingwell, J.: Hazard from volcanic ash, *Nature*, 354, p. 25, 1991.
- Prata, F., Bluth, G., Rose, B., Schneider, D., and Tupper, A.: Failures in detecting volcanic ash from a satellite-based technique – Comments, *Remote Sens. Environ.*, 78, 341–346, 2001.
- Prata, A., Rose, W., Self, S., and O'Brien, D.: Global, long-term sulphur dioxide measurements from the TOVS data: a new tool for studying explosive volcanism and climate, *Geophys. Monogr.*, 139, 75–92, 2003.
- READY: Real-time Environmental Applications and Display sYstem, , Air Resources Laboratory, NOAA, <http://ready.arl.noaa.gov/READY.php>, last access: January 2011.
- Realmuto, V., Abrams, M., Buongiorno, M., and Pieri, D.: The use of multispectral thermal infrared image data to estimate the sulfur-dioxide flux from volcanoes – A case-study from Mount Etna, Sicily, July 29, 1986, *J. Geophys. Res.-Sol. Ea.*, 99, 481–488, 1994.
- Rix, M., Valks, P., Hao, N., van Geffen, J., Clerbaux, C., Clarisse, L., Coheur, P.-F., Loyola R, D. G., Erbetseder, T., Zimmer, W., and Emmadi, S.: Satellite Monitoring of Volcanic Sulfur Dioxide Emissions for Early Warning of Volcanic Hazards, *IEEE J. Sel. Top. Appl.*, 2, 196–206, doi:10.1109/JSTARS.2009.2031120, 2009.
- Romero, R. (Ed.): The International Airways Volcano Watch (IAVW). Proceedings of 2nd International Conference on Volcanic Ash and Aviation Safety, Virginia, USA, 2004.
- Rose, W., Delene, D., Schnelder, D., Bluth, G., Krueger, A., Sprod, I., Mckee, C., Davies, H., and Ernst, G.: Ice in the 1994 Rabaul eruption cloud – implications for volcanic hazard and atmospheric effects, *Nature*, 375, 477–479, 1995.
- Schumann, U., Weinzierl, B., Reitebuch, O., Schlager, H., Minikin, A., Forster, C., Baumann, R., Sailer, T., Graf, K., Mannstein, H., Voigt, C., Rahm, S., Simmet, R., Scheibe, M., Lichtenstern, M., Stock, P., Rüba, H., Schäuble, D., Tafferner, A., Rautenhaus, M., Gerz, T., Ziereis, H., Krautstrunk, M., Mallaun, C., Gayet, J.-F., Lieke, K., Kandler, K., Ebert, M., Weinbruch, S., Stohl, A., Gasteiger, J., Gro, S., Freudenthaler, V., Wiegner, M., Ansmann, A., Tesche, M., Olafsson, H., and Sturm, K.: Airborne observations of the Eyjafjalla volcano ash cloud over Europe during air space closure in April and May 2010, *Atmos. Chem. Phys.*, 11, 2245–2279, doi:10.5194/acp-11-2245-2011, 2011.
- Simpson, J., Hufford, G., Pieri, D., and Berg, J.: Failures in detecting volcanic ash from satellite-based technique, *Remote Sens. Environ.*, 72, 191–217, 2000.
- Solomon, S., Schmeltekopf, A. L., and Sanders, R. W.: On the interpretation of zenith sky absorption measurements, *J. Geophys. Res.*, 92, 8311–8319, 1987.
- Thomas, H. E. and Prata, A. J.: Sulphur dioxide as a volcanic ash proxy during the April-May 2010 eruption of Eyjafjallajökull Volcano, Iceland. *Atmos. Chem. Phys.*, 11, 6871–6880, doi:10.5194/acp-11-6871-2011, 2011.
- Thomas, H. E. and Watson, I. M.: Observations of volcanic emissions from space: current and future perspectives, *Nat. Hazards*, 54, 323–354, doi:10.1007/s11069-009-9471-3, 2010.
- Tupper, A., Textor, C., Herzog, M., Graf, H.-F., and Richards, M. S.: Tall clouds from small eruptions: the sensitivity of eruption height and fine ash content to tropospheric instability, *Nat. Hazards*, 51, 375–401, doi:10.1007/s11069-009-9433-9, 2009.
- Voigt, S., Orphal, J., Bogumil, K., and Burrows, J.: The temperature dependence (203–293 K) of the absorption cross sections of O₃ in the 230–850 nm region measured by Fourier-transform

- spectroscopy, *J. Photoch. Photobio. A*, 143, 1–9, 2001.
- Wagner, T., Burrows, J. P., Deutschmann, T., Dix, B., von Friedeburg, C., Frie, U., Hendrick, F., Heue, K.-P., Irie, H., Iwabuchi, H., Kanaya, Y., Keller, J., McLinden, C. A., Oetjen, H., Palazzi, E., Petritoli, A., Platt, U., Postlyakov, O., Pukite, J., Richter, A., van Roozendaal, M., Rozanov, A., Rozanov, V., Sinreich, R., Sanghavi, S., and Wittrock, F.: Comparison of box-air-mass-factors and radiances for Multiple-Axis Differential Optical Absorption Spectroscopy (MAX-DOAS) geometries calculated from different UV/visible radiative transfer models, *Atmos. Chem. Phys.*, 7, 1809–1833, doi:10.5194/acp-7-1809-2007, 2007.
- Wen, S. and Rose, W.: Retrieval of sizes and total masses of particles in volcanic clouds using AVHRR bands 4 and 5, *J. Geophys. Res.*, 99, 5421–5431, 1994.
- Zehner, C. (Ed.): *Monitoring Volcanic Ash from Space. Proceedings of the ESA-EUMETSAT workshop on the 14 April to 23 May 2010 eruption at the Eyjafjöll volcano, South Iceland*, vol. ESA Publikation STM-280, ESA, ESA, Frascati, Italy, doi:10.5270/atmch-10-01, 2010.
- Zhang, Y. and Johansson, M.: *MobileDOAS*, Department of Earth and Space Sciences, Chalmers University of Technology, Gothenburg, Sweden, 2007.